



Supramolecular Assembly Interceded by C-H...O Hydrogen Bonds and Nitro... π (arene) Interactions of Antibacterial 4-Methyl-(2-nitro benzylidene)aniline using DFT and its Spectral Studies

R. MINI¹, T. JOSELIN BEAULA², P. MUTHURAJA³ and V. BENA JOTHY^{1,*}

¹Department of Physics, Women's Christian College (Affiliated to Manonmaniam Sundaranar University, Tirunelveli), Nagercoil-629001, India

²Department of Physics, Malankara Catholic College (Affiliated to Manonmaniam Sundaranar University, Tirunelveli), Kaliakkavilai-629153, India

³P.G. and Research Department of Chemistry, Sri Ramakrishna Mission Vidyalaya, College of Arts and Science, Coimbatore-641020, India

*Corresponding author: E-mail: benaezhil@yahoo.com

Received: 16 October 2019;

Accepted: 15 December 2019;

Published online: 29 April 2020;

AJC-19833

4-Methyl-(2-nitrobenzylidene)aniline (MNBA) was grown and its structural as well as spectral analyses (FT-IR, FT-Raman, UV and NMR) using experimental and DFT computations were performed to understand its biological applications. Stability of molecule, charge delocalization, charge analysis and charge transfer interactions had been explored to examine the structural analysis. Docking studies also suggested that 4-methyl-(2-nitrobenzylidene)aniline exhibit antibacterial activity. Supramolecular assembly of 4-methyl-(2-nitrobenzylidene)aniline molecule was interceded by C-H...O hydrogen bonds and nitro... π (arene) interactions.

Keywords: 4-Methyl-(2-nitrobenzylidene)aniline, Natural bond orbital, Structural analysis.

INTRODUCTION

Development of biologically active molecules require a multidisciplinary effort by combining organic chemistry, crystal growth, material science and physics. Organic base aniline is generally used to make dyes, explosives and drugs. In medicinal and biological chemistry fields, benzylidene anilines possess an important class of Schiff bases. It may also possess significant anticancer and anti-inflammatory activities which act as reagents for various stereoselective organic synthesis [1]. Benzylidene aniline has the relieving property for inflammations in the warm-blooded animals and also consists of various pharmaceutical compositions. It is also used for the treatment of radiation induced by the topical administration. Benzylidene aniline derivatives exhibit effective sun screening property [2].

Azomethine group enables attachment and extension of π -donating groups [3]. Cyano (CN) group, gets adsorbed on the metal surfaces easily due to planarity of π -bonding orbitals and electrons from the attached electronegative atoms [4]. Hydrogen bonding interaction results in the formation of a bridge of the sort C-H...O and nitro... π interactions causing shift following bond stretching or contraction which compile

antibacterial activity. In ¹H NMR, a substituent behaviour of NMR chemical shift centre has an application of using as a probe for the electronic properties of delocalized π -system of benzylidene aniline [5]. The dual replacement of parameters in azomethine, ¹³C NMR shift gave important insight into the special behaviour of CN group as a substituent. The CN group inductively has a strong electron-withdrawing group, whereas mesomerically it also have the strong electron donating group [6]. In benzoic complexes, the donor-acceptor groups are connected *via* varying carbon-carbon single and double bonds. Benzylidene anilines are isoelectronic which regards their π -electronic structure; their properties can be strongly different [7]. Schiff bases have been contemplated like versatile ligands which provide probability to the design metal complexes for helpful in biological activities. Several Schiff bases exhibit biological activities such as anti-fungal, antibacterial, antitumor, anti-inflammatory and antipyretic activities [8-10]. The antibacterial activity has been analyzed more than antifungal activity because bacterium can obtain resistance to antibiotics through biochemical and morphological modifications [11,12]. In organic syntheses, a formation of carbon-nitrogen double bond is important and the Schiff bases can be synthesized from an amine and a carbonyl compound [13].

Quantum chemical computations has been carried out at B3LYP / 6-311G(d) basis level to obtain optimized structure which provides information about structural, spectral and electronic properties. Various spectral characterizations using UV-visible, IR, Raman, ^1H & ^{13}C NMR techniques together with X-ray diffraction analysis have been used to elucidate the structure of 4-methyl-(2-nitrobenzylidene)aniline (MNBA). NBO analyses were carried out to identify the intra and intermolecular interactions. The reactive sites of the title molecule were identified by the molecular electrostatic potential analysis (MEP) and the group contribution of molecule was carried out by density of state (DOS) analysis.

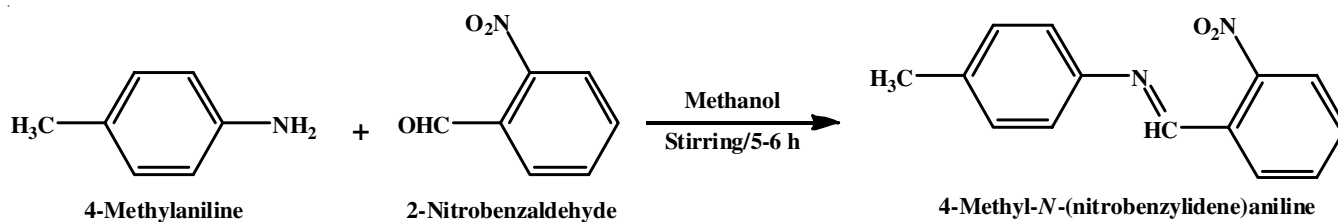
EXPERIMENTAL

Synthesis of 4-methyl-(2-nitrobenzylidene)aniline (MNBA): Slow evaporation solution growth technique was used for the growth of MNBA crystal. Analytical grades of 4-methylaniline and 2-nitrobenzaldehyde were taken in 1:1 stoichiometric proportions and dissolved in methanol thoroughly using mechanical stirrer for 5-6 h. Clear brown solution was obtained and filtered off using Whatman 40 grade filter paper to remove the suspended impurities (**Scheme-I**). The filtrate was kept aside without any mechanical shake in a dust free environment at room temperature. Bright brown 4-methyl-(2-nitrobenzylidene)aniline (MNBA) single crystal (Fig. 1) was obtained within 4-5 days and collected from the mother liquor. The harvested MNBA crystals were recrystallized from ethanol to get superior quality crystals.



Fig. 1. Photograph of the grown MNBA crystal

Characterization: Powder XRD data were collected in a Bruker AXS instrument using $\text{CuK}\alpha$ radiation ($\lambda = 1.5406 \text{ \AA}$). Fourier transform infrared spectrum of MNBA crystal was recorded using Shimadzu IR-affinity 1 instrument in the region



Scheme-I: Synthetic reaction of 4-methyl-(2-nitrobenzylidene)aniline (MNBA)

4000-400 cm^{-1} by KBr pellet technique. FT-Raman spectral studies was carried out using Bruker RFS 27 stand alone FT-Raman spectrometer with laser source Nd:YAG 1064 nm in the spectral range of 4000-500 cm^{-1} at room temperature. NMR spectra was obtained using Bruker NMR spectrometer using TMS as an internal standard. Thermal stability of the crystal was examined using Thermogravimetric analysis. UV-visible absorption spectrum of MNBA was recorded using methanol solvent, JASCO UV-Vis spectrophotometer in the spectral region of 200-400 nm.

Computational studies: DFT calculations were performed using Gaussian 09 software [14] to obtain optimized geometry, NBO analysis, HOMO-LUMO energy gap and charge analyses at B3LYP/6-31G(d,p) level. Normal mode characterization was performed with MOLVIB 7.0 program [15,16]. To improve agreement between experimental and theoretical frequencies, theoretical values were scaled using SQMFF procedure [17, 18]. Electronic properties were determined by TD DFT approach, by taking solvent effect into account [19-22] where the important quantities were deduced from ionization potential and electron affinity values [23-25]. GIAO method was used to calculate NMR isotropic shielding [26,27] and AutoDock4 was used to perform docking studies [28].

RESULTS AND DISCUSSION

PXRD analysis: Purity and crystalline nature of MNBA crystal had been confirmed by recording powder X-ray diffraction pattern. Powder X-ray diffraction pattern is shown in Fig. 2. The well-defined and sharp Bragg peaks at specific 2θ angles were in agreement with the theoretical data. All the observed reflections were indexed by using CRYSFIRE software package. Cell parameters and calculated 2θ for MNBA are presented in Table-1. The given data clearly confirmed the successful formation of MNBA.

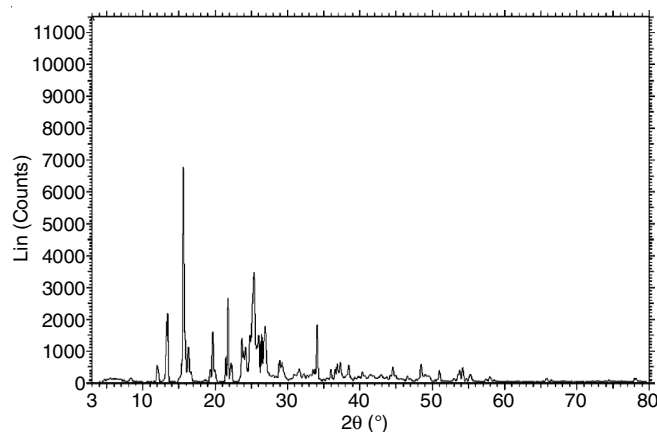


Fig. 2. Powder X-ray Diffraction spectrum of MNBA compound

Unit cell parameters			2 θ	2 θ	'd'
h	k	l	Observed	Calculated	Observed
0	0	1	11.921	11.909	7.4179
1	2	0	13.321	13.324	6.6412
2	2	0	15.516	15.456	5.7064
2	1	1	16.209	16.222	5.4639
2	2	1	19.584	19.556	4.5293
4	0	1	21.290	21.697	4.0940
2	3	1	24.130	24.144	3.6853
5	2	0	25.959	25.960	3.4296
2	1	2	26.371	26.412	3.3770
2	4	0	26.827	26.827	3.3206

Optimized geometry: An optimized structure of MNBA is shown in Fig. 3 and the geometrical parameters have been listed in Table-2. Phenyl rings were established to be planar within 1° twist. Shortening of bond length C3-N4 (1.407 Å) shorter than C-N single (1.465 Å) bond exposes the effect of resonance in nitro group of molecule nonetheless C-N double-bond length C1-N8 (1.289 Å) is longer than the normal C=N bond (1.279 Å), exposing the effect of protonation of azomethine [29]. Asymmetry in phenyl rings exo-angles C4-C3-C9 and C2-C3-N9 were 117.8579° and 121.72° were deviated from the normal value 120° which is due to the substitution of nitro group. Endocyclic angles C12-C11-C10 (118.4°) and C4-C3-N1 (114.7°) get shortened in addition to lengthening of exo-cyclic angles C10-C11-C14 (121.3°) and C4-C3-C2 (121.7°) at the donor and acceptor side, respectively. This asymmetry of angles clearly proves the charge-transfer interaction within the system, nature of electron donor methyl group, acceptor nitro group and also confirms the push-pull nature of those two groups and hence this class of system is known as push-pull chromophore. Large reduction in the endocyclic angles C3-C2-C7 (116.8°) and C13-C8-C9 (118.6°) of two phenyl rings at the junction of azomethine linkage obviously proves the conjugation of two aromatic rings with C1=N2.

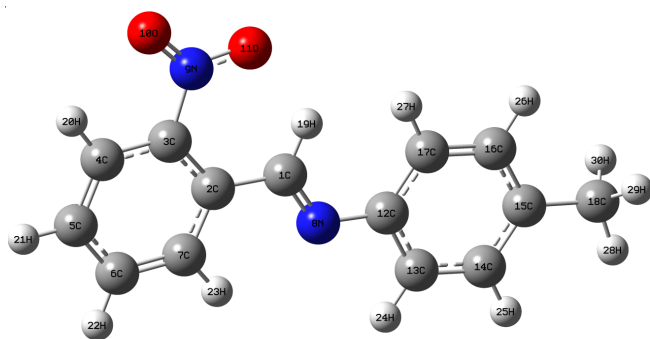


Fig. 3. Optimized molecular structure of synthesized MNBA molecule

An increase in the bond length values of C2-C3 (1.402 Å), C2-C7 (1.398 Å), C8-C9 (1.394 Å) and C8-C13 (1.398 Å) compared to other CC lengths of aromatic rings also confirms the hyper-conjugation of phenyl rings through C2-C1=N2-C8 path, which was further evident from the partial double bond nature of C1-N2 (1.281 Å). All these facts clearly revealed the intramolecular charge transfer taking place within MNBA compound. Bond length values of N1-O1 (1.277 Å), N1-O2

(1.281 Å) lie between N-O single and N=O double bond length values, indicating an electron delocalization within NO₂ group. Optimized geometry of MNBA compound revealed that NO₂ and CH₃ groups were lying parallel with respect to benzene ring, which is recognized from their torsion angle values C4-C3-N1-O2 (-180°), C2-C3-N1-O1 (180°) and C10-C12-C11-C14 (179.9°).

Azomethine linkage forms a dihedral angle of 180° (C3-C2-C1=N2, C1=N2-C8-C9) with aromatic ring of 2-nitrobenzaldehyde moiety and 4-methylaniline moiety, which is the clear proof for the planarity that exists between phenyl ring and azomethine group. From the aforementioned bond length, bond angle and torsion data, it is clearly understood that charge transfer interaction is taking place from electron donor to acceptor moiety through imine linkage. This intermolecular charge transfer in the molecule generates two different molecular domains within π -conjugated bridge. One of the domains has partial quinonoid character and the other has an almost pure aromatic character. So this π -electron cloud movement from electron donor to acceptor is capable of highly polarizing the molecule through the single-double path, when it changes from the benzenoid form into the quinonoid form. Bond length of C1-H19...O11, C4-H20...O10 and C13-H24...N8 were 2.2276 Å, 2.3690 Å and 2.43486 Å, respectively which are shorter than van der Waals radii, confirming the presence of C-H...O hydrogen bonds and NO₂... π (arene) interactions.

Natural bond orbital analysis: Second order perturbation theory analysis and natural hybrid orbital in NBO basis are shown in Table-3. Inter and intra-molecular hyper-conjugative interactions n1(O11) with σ^* (C1-H19), n3(O11) with σ^* (C1-H19), n1(N8) with σ^* (C1-H19) and σ^* (C7-H23) have stabilization energies 0.63, 0.99, 12.02 and 0.89 kcal/mol which revealed the presence of C-H...O and nitro... π (arene) hydrogen bonds interactions. Natural hybrid orbital of n2(O10), n2(O11) and n3(O11) have low occupation numbers (1.89637, 1.89943 and 1.43979), substantial higher energy orbital π -characters (99.82, 99.66 and 99.25 %) have lower energies (-0.29439, -0.29696 and -0.28114 a.u.) and n1(O10), n1(O11) and n2(N8) have high occupation numbers (1.98127, 1.97919, 1.89909) with energies, -0.80175, -0.80232, -0.34386 a.u. with lower energy orbital π -characters (25.08, 25.05, 72.50 %). From these results, it can be inferred that pure *p*-type lone pair orbital participates in electron donation which is very close to the σ^* (N-C) orbital for n2(O10) \rightarrow σ^* (N-C), n2(O11) \rightarrow σ^* (N-C) and n2(O11) \rightarrow σ^* (N-C) orbital for n1(N8) \rightarrow σ^* (C-C), n1(N6) \rightarrow σ^* (C-H) interactions in MNBA compound.

Vibrational analysis: Vibrational spectral assignment of MNBA molecule fundamentals has been done based on normal coordinate analysis. Fundamental band frequencies from experimental IR and Raman spectra were scaled wavenumbers together with the normal mode descriptions (Table-4). FT-IR and FT-Raman spectra were exposed as overlaid with the corresponding replicated spectra for optical comparison (Fig. 4).

Phenyl ring vibrations: Selection rule for *ortho*-disubstituted phenyl ring allows four C-H stretching vibrations, viz. 2, 7b, 20a and 20b in the range 3120-3010 cm⁻¹ [30]. Mode 2 was observed in IR as weak band at 3095 cm⁻¹, while mode 20b was observed as a weak band at 3061 cm⁻¹. In Raman, this

TABLE-2
OPTIMIZED BOND LENGTHS (Å), BOND ANGLES (°) AND DIHEDRAL
ANGLES (°) OF MNBA COMPOUND BY B3LYP/6-311G(d) BASIS SETS

Bond length	(Å)	Bond angle	(°)	Dihedral angle	(°)
C1- C2	1.4782	C2-C1-N8	121.3912	N8-C1-C2-C3	-129.8934
C1-N8	1.2816	C2-C1-H19	113.9998	N8-C1-C2-C7	51.5171
C1-H19	1.0901	N8-C1-H19	124.6007	H19-C1-C2-C3	49.1331
C2-C3	1.4105	C1-C2-C3	121.6808	H19-C1-C2-C7	-129.48
C2-C7	1.4068	C1-C2-C7	119.6064	C2-C1-N8-C12	178.0049
C3-C4	1.396	C3-C2-C7	118.6987	H19-C1-N8-C12	-0.8859
C3-N9	1.4736	C2-C3-C4	120.4195	C1-C2-C3-C4	-120.4195
C4-C5	1.3896	C2-C3-N9	121.7200	C1-C2-C3-N9	2.4364
C4-H20	1.0825	C4-C3-N9	117.8579	C7-C2-C3-C4	0.603
C5-C6	1.3983	C3-C4-C5	119.7155	C7-C2-C3-N9	-178.9361
C5-H21	1.0851	C3-C4-H20	120.0448	C1-C2-C7-C6	177.6668
C6-C7	1.3893	C5-C4-H20	120.2402	C1-C2-C7-H23	-1.9693
C6-H22	1.0857	C4-C5-C6	120.2043	C3-C2-C7-C6	-0.9899
C7-H23	1.0839	C4-C5-H21	119.5908	C3-C2-C7-H23	179.374
N8-C12	1.4064	C6-C5-H21	120.2028	C2-C3-C4-C5	-0.1383
N9-O10	1.2303	C5-C6-C7	120.1407	C2-C3-C4-H20	-179.9547
N9-O11	1.2333	C5-C6-H22	120.008	N9-C3-C4-C5	179.4183
C12-C13	1.405	C7-C6-H22	119.8446	N9-C3-C4-H20	-0.3981
C12-C17	1.4047	C2-C7-C6	120.8143	C2-C3-N8-O10	-178.9258
C13-C14	1.3893	C2-C7-H23	119.1098	C2-C3-N9-O11	1.2265
C13-H24	1.0854	C6-C7-23	120.0748	C4-C3-N9-O10	1.5238
C14-C15	1.4039	C1-N8-C12	120.6073	C4-C3-C9-O11	-178.3239
C14-H25	1.0873	C3-N9-O10	118.4439	C3-C4-C5-C6	0.0443
C15-C16	1.4004	C3-N9-O11	120.0993	C3-C4-C5-H21	179.5238
C15-C18	1.5098	O10-N9-O11	121.4566	H20-C4-C5-C6	179.8603
C16-C17	1.3932	N8-C12-C13	118.4269	H20-C4-C5-H21	-0.6601
C16-H26	1.087	N8-C12-C17	122.9286	C4-C5-C6-C7	-0.4265
C17-H27	1.0857	C13-C12-C17	118.5508	C4-C5-C6-H22	-179.4894
C18-H28	1.096	C12-C13-C14	120.2907	H21-C5-C6-C7	-179.9028
C18-H29	1.0964	C12-C13-H24	120.132	H21-C5-C6-H22	1.0342
C18-H30	1.0932	C14-C13-H24	119.5141	C5-C6-C7-C2	0.9108
		C13-C14-C15	120.9724	C5-C6-C7-H23	-179.4566
		C13-C14-H25	119.3471	H22-C6-C7-C2	179.9753
		C15-C14-H25	119.6744	H22-C6-C7-H23	-0.3921
		C14-C15-C16	118.9195	C1-N8-C12-C13	147.6777
		C14-C15-C18	121.0881	C1-N8-C12-C17	-35.8963
		C16-C15-C18	119.9881	N8-C12-C13-C14	177.2653
		C15-C16-C17	120.8682	N8-C12-C13-H24	-2.9688
		C15-C16-H26	119.6137	C17-C12-C13-C14	0.6802
		C17-C16-H26	119.5181	C17-C12-C13-H24	-179.5539
		C12-C17-C16	120.3914	N8-C12-C17-C16	-176.3624
		C12-C17-H27	119.9305	N8-C12-C17-H27	1.7952
		C16-C17-H27	119.6526	C13-C12-C17-C16	0.0594
		C15-C18-H28	109.7335	C13-C12-C17-H27	178.2171
		C15-C18-H29	108.5571	C12-C13-C14-C15	-0.8617
		C15-C18-H30	109.5074	C12-C13-C14-H25	179.957
		H28-C18-H29	109.443	H24-C13-C14-C15	179.3708
		H28-C18-H30	109.380	H24-C13-C14-H25	0.2756
		H29-C18-H30	109.306	C13-C14-C15-C16	0.2864
				C13-C14-C15-C18	179.5304
				H25-C14-C15-C16	179.3787
				H25-C14-C15-C18	1.3773
				C14-C15-C16-C17	0.4637
				C14-C15-C16-H26	179.6215
				C18-C15-C16-C17	178.7888
				C18-C15-C16-H26	1.126
				C14-C15-C18-H28	22.3089
				C14-C15-C18-H29	97.2589
				C14-C15-C18-H30	143.4721
				C16-C15-C18-H28	158.4551
				C16-C15-C18-H29	81.9771
				C16-C15-C18-H30	37.2919
				C15-C16-C17-C12	0.6346
				C15-C16-C17-H27	178.7974
				H26-C16-C17-C12	179.4504
				H26-C16-C17-H27	1.2877

TABLE-3
SECOND ORDER PERTURBATION THEORY ANALYSIS OF
FOCK MATRIX IN NBO BASIS OF MNBA COMPOUND

Donor (i)	ED(i)/energy (e)	S %	P %	Acceptor (j)	E(2) (kcal mol ⁻¹)
n1(O11)	1.97919 -0.80232	74.94	25.05	$\sigma^*(C_1-H_{19})$	0.63
n2(O11)	1.89943 -0.29696	0.25	99.99	$\sigma^*(C_3-N_9)$	11.81
n3(O11)	1.43979 -0.28114	0.54	99.25	$\sigma^*(C_1-H_{19})$	0.99
n1(N8)	1.89909 -0.34386	27.37	72.50	$\sigma^*(C_1-H_{19})$ $\sigma^*(C_7-H_{23})$	12.02 0.89
n1(O10)	1.89909 -0.80175	74.92	25.08	$\sigma^*(C_3-N_9)$	4.24
n2(O10)	1.89637 -0.29439	0.08	99.82	$\sigma^*(N_9-O_{11})$	19.39

TABLE-4
VIBRATIONAL ASSIGNMENTS OF MNBA COMPOUND
BY NORMAL COORDINATE ANALYSIS

Observed fundamentals (cm ⁻¹)		Selective scaled B3LYP/6-31G(d) force field	
IR	Raman	V _{cal} (cm ⁻¹)	Assignment with PED (≥ 100 %)
	3125w	3172	$\nu_{OS}CH_3$ (71), $\nu_{IS}CH_3$ (29)
	3112w	3140	$\nu_{IS}CH_3$ (71), $\nu_{OS}CH_3$ (29)
		3129	ν_{CHR1} (99)
		3113	ν_{CHR1} (99)
		3098	ν_{CHR1} (99)
3095w		3093	ν_{CHR2} (96)
		3089	ν_{CHR2} (95)
		3080	ν_{CHR1} (99)
		3063	ν_{CHR2} (95)
3061w	3060w	3061	ν_{CHR2} (96)
		2970	$\nu_{SS}CH_3$ (99)
	2968w	2968	ν_{SCH} (98)
		1935	ν_{CNM} (72), ν_{CHR} (13)
		1812	ASD2 (25), ASDO2 (21), ν_{CC2} (15), ν_{CC} (13), $\nu_{AS}NO_2$ (11)
		1806	ASD2 (29), ASDO2 (27), ν_{CC2} (20)
1792vs		1770	ν_{CC2} (74)
		1762	ν_{CC1} (49), β_{CH1} (18)
1707vs		1738	ν_{CC1} (50), β_{CH1} (12)
		1697	ASD2 (48), ν_{CC2} (20), β_{CH2} (20)
		1641	β_{CHR1} (44), ν_{CC1} (32)
	1620m	1625	$\nu_{AS}CH_3$ (78)
		1612	$\nu_{ASO}CH_3$ (91)
	1609w	1607	β_{CHR1} (48), ν_{CC1} (32)
	1582vs	1580	ν_{CC2} (32), β_{CHR2} (24), ν_{CHR} (15)
	1553w	1574	ν_{CC2} (30), ν_{CHR} (19), β_{CH2} (14), ν_{CC1} (13)
1537w		1559	$\nu_{SS}NO_2$ (45), ν_{CN} (16), $\nu_{SD}CO_2$ (15), ν_{CHR} (11), $\nu_{AS}NO_2$ (10)
		1547	$\nu_{SD}CH_3$ (86), $\nu_{AS}NO_2$ (13)
		1527	ν_{CC2} (55), ν_{CC1} (28)
		1510	ν_{CC1} (44), ν_{CC2} (30)
1445s		1452	β_{CHR2} (74)
	1434w	1412	β_{CHR1} (43), ν_{CC1} (12)
1398s	1399w	1397	ASD2 (45), TD2 (17), ν_{CN} (15)
	1325w	1320	TD2 (33), ASD2 (24), ν_{CC} (15), ν_{CC2} (11)

	1312	ν_{CC} (24), β_{CH1} (23), ν_{CC1} (23)
	1295	β_{CHR2} (44), ASD2 (28), CC2 (15)
	1279s	1282 β_{CHR1} (77), ν_{CC1} (18)
1224w	1255	ν_{CC1} (36), β_{CHR1} (34), ν_{CN} (14)
1170s	1229	β_{CHR2} (59), ν_{CC2} (32)
	1162w	1161 TD1 (30), ν_{CC1} (18), ν_{CN} (14), β_{CH1} (13)
	1126s	1135 ν_{CC1} (63), β_{CHR1} (19)
1124w	1132	PK2 (33), $\nu_{R}CH_3$ (25), ATO2 (15), $\nu_{RO}CH_3$ (11)
1096vs	1090	TD2 (47), ASD2 (19), $\nu_{RO}CH_3$ (13), ν_{CC2} (11)
1076w	1080	TD2 (61), ASD2 (20)
	1011	GCHR1 (64), PK1 (10)
	998	ω_{CH} (26), ATO2 (20), PK2 (16), GCH1 (16)
	981	GCHR1 (78)
971w	978	ATO2 (22), TD2 (21), PK2 (18)
	956w	967 ATO2 (57), AT2 (24), GCH2 (14)
953s	959	PK2 (51), GCHR2 (19), ATO2 (18)
939m	942	$\nu_{SD}CO_2$ (45), TD1 (22), $\nu_{SS}NO$ (11)
929m	905	GCHR1 (58), ASDO2 (10)
893s	898	ASDO2 (30), ASD2 (25), ν_{CC2} (11)
	862vs	848 GCHR2 (52), ATO2 (25), $\nu_{AS}CN$ (14)
	835w	839 NO_2DF (37), GCHR2 (26), AT2 (19), PK2 (11)
		823 ASD2 (66), τ_{D2} (19)
		807 GCHR1 (41), GCO2 (22), GCN1 (15), PK1 (10)
	751w	761 NO_2SC (23), ATO2 (20), GCH1 (17), PK1 (13)
	730w	733 PK2 (35), ATO2 (33)
		726 PK2 (50), ATO2 (47)
712w	713	PK2 (47), ATO2 (43)
667s	670	ASDO2 (52), ASD2 (15)
640s	660	ASDO2 (50), ASDO1 (11)
602s	616	PK2 (29), ATO2 (17), ASDO1 (13)
	553w	561 PK2 (39), AT2 (32), NO_2ROCK (12)
		547 AT2 (24), β_{CN2} (10)
531w	518	ASDO2 (47), ASD2 (42)
523vs	502	AT2 (42), ATO2 (16)
514vs	496w	433 AT1 (23), ATO2 (18), AT2 (13), GCN1 (11), ATO1 (10)
	423w	422 ATO2 (54), AT2 (45)
		408 ATO2 (52), AT2 (37)
		386 ATO2 (42), AT2 (17), ASDO2 (10)
	377s	364 ATO2 (50), PK2 (28)
		324 ASD2 (26), β_{CN1} (13), ASDO2 (12), $XCPCC2$ (11)
	273w	293 ATO1 (23), AT2 (15)
	231w	241 AT2 (30), PK2 (21)
		210 ASD2 (49), ASDO2 (22)
		163 AT2 (54), ATO2 (19)
		143 τ_{CN1} (29), ASD2 (14)
	121vvs	114 AT2 (37), ATO2 (28)
		66 ATO2 (27), AT2 (27), τ_{NO_2} (24)
		52 β_{CNC} (21), β_{CN2} (15), τ_{CN2} (13), τ_{CH} (10)
		45 ATO (26), ATO2 (22)
		28 τ_{CH} (41), τ_{NO_2} (18)
		24 τ_{CH_3} (44), GCC2 (17), PK2 (14)
		20 τ_{CH_3} (27), τ_{CH} (23), GCC2 (15)

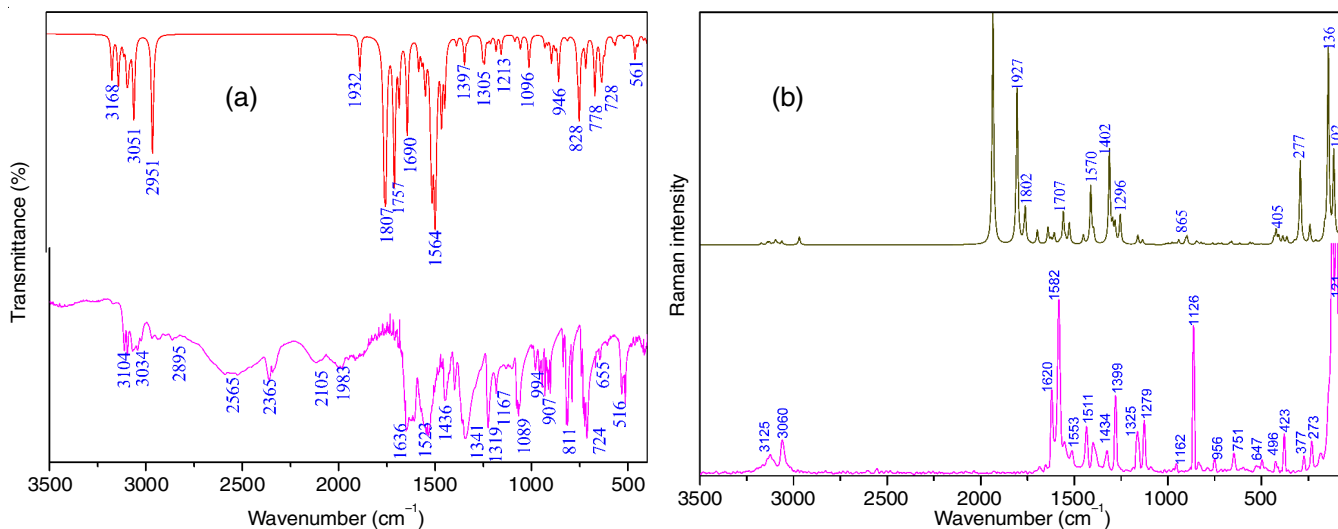


Fig. 4. Experimental and simulated FT-IR (a) and FT-Raman (b) spectra of MNBA compound

mode was observed at 3060 cm⁻¹ and the scaled value was at 3061 cm⁻¹. These modes were generally pure and their contributions are calculated as 99 % PED. There were six C-C stretching vibrations (**8a**, **8b**, **19a**, **19b** and **14**) and considered as more substituent dependent. The expected range of degenerate mode **8a** of *ortho*-disubstituted ring was 1609-1565 cm⁻¹ and **8b** extends from 1625-1586 cm⁻¹ with **8a** smaller than **8b**. Mode **8b** was observed as strong band in Raman at 1792 cm⁻¹ and in addition strong band at 1707 cm⁻¹ in Raman is assigned to mode **8a**, which is coupled with C-H bending mode. Blue shift of phenyl ring C-C stretching mode is due to steric interaction that induces effective conjugation and charge carrier localization resulting in phenyl ring twisting. Mode **19a** was observed as strong band at 1582 cm⁻¹ in IR spectrum. This was coupled with C-H bending mode. Mode **19b** mode appeared as a weak band at 1553 cm⁻¹. In these vibrations, there was considerable percentage of C-H bend character. This arises as the hydrogen and carbon move oppositely during C-C stretching. The increased in intensities of these bands can be contributed to the methyl substituent having electron-donor properties.

Another important ring mode is the in-plane C-H bending. The small amount of C-C stretch interaction associated with this mode usually appears in the region 1300-1100 cm⁻¹. In IR, weak band was observed at 1224 cm⁻¹ and in Raman, a strong band was observed at 1279 cm⁻¹ correspond to this vibration. Normal mode was active in IR as a weak intense band at 1224 cm⁻¹ and as a strong band in Raman spectrum at 1126 cm⁻¹. The C-H out-of-plane bending vibrations were generally observed in the region 1000-675 cm⁻¹. These modes were designated as *gauche* in internal coordinates definition. They were identified as medium IR bands at 929 cm⁻¹ and as weak Raman bands at 751, 835 and 956 cm⁻¹.

Methyl vibrations: Methyl group contributes significantly to the vibrational spectra of MNBA molecule. A downshift caused by electronic effects in symmetric and asymmetric stretching modes of methyl group attached to benzene ring was expected near 2925 and 2865 cm⁻¹, respectively. The weak band in Raman spectrum at 2968 cm⁻¹ was due to symmetric stretching mode. This can direct to changing polarizability and dipole moment due to electron delocalization, causing

changes in the intensity of IR spectrum. This indicates that the hydrogen atoms of methyl group were directly involved in donation of electronic change. Thus, hyperconjugation and back donation of methyl group with the aromatic ring system caused a changes in the intensity of IR spectrum clearly indicates that methyl hydrogens were directly involved in the donation of electronic change [31]. Methyl group yields to the strengthening of C-H bond which is clearly seen in the experimental value of C-H bond length (Table-4). The methyl group's out-of-plane bending mode was expected near 1460 cm⁻¹ and the methyl group out-mode was coupled with CH₃ in-plane bending mode and observed as off-plane bending as a strong band at 1445 cm⁻¹ in IR spectrum with major PED contribution of 99 %. Torsions and other modes are also shown in Table-4.

Azomethine vibrations: The C-H stretching vibrations were observed in the region 3100-3000 cm⁻¹ and these vibrations were not affected by the nature and position of substituent. In MNBA, the symmetric stretching vibrations were observed at 3061 cm⁻¹ in FT-IR and 3060 cm⁻¹ in FT-Raman. The C-N stretching vibration was strongly split into an asymmetric and a symmetric component. C-N stretching vibration of aromatic rings was observed at 1162 cm⁻¹ in Raman spectrum. A downshift of this vibration was a resonance structure of *ortho*-disubstituted benzaldehyde.

The C=N stretching mode helps in the evaluation of bonding configuration around amino N atom and the electronic distribution of aromatic amine compounds. C=N stretching is generally expected in the region 1670-1600 cm⁻¹, but in MNBA molecule, C=N stretching band was observed at 1610 cm⁻¹. Charge transfer interaction between the donor and acceptor through -C=N-C skeleton causes downward shift of C=N stretching frequency.

NO₂ Vibrations: A NO₂ group was involved in the intramolecular charge-transfer, intermolecular hydrogen bond and dipole-dipole interactions. In aromatic nitro compounds, asymmetric and symmetric vibrations of NO₂ group gives rise to strong bands at 1550-1510 and 1365-1335 cm⁻¹, respectively [32]. A very strong band observed at 1582 cm⁻¹ which had been assigned to the NO₂ asymmetric stretching vibration. Intensity enhancement of these wavenumbers is due to the conju-

TABLE-6
UV-VISIBLE EXCITATION ENERGY AND OSCILLATOR STRENGTH OF SYNTHESIZED MNBA COMPOUND

Energy (cm ⁻¹)	Wavelength (nm)		Oscillator strength	Symmetry	Major contributes
	Cal	Exp			
23446	426	440	0.3768	Singlet-A	HOMO → LUMO (99 %)
26522	377	–	0.0002	Singlet-A	H-2 → LUMO (91 %)
29850	334	–	0.0057	Singlet-A	H-1 → LUMO (98 %)
31551	316	–	0.0001	Singlet-A	H-5 → LUMO (73 %); H-2 → L+1 (18 %)
31636	316	–	0.4412	Singlet-A	HOMO → L+1 (86 %)
33251	300	–	0.0876	Singlet-A	H-3 → LUMO (85 %)

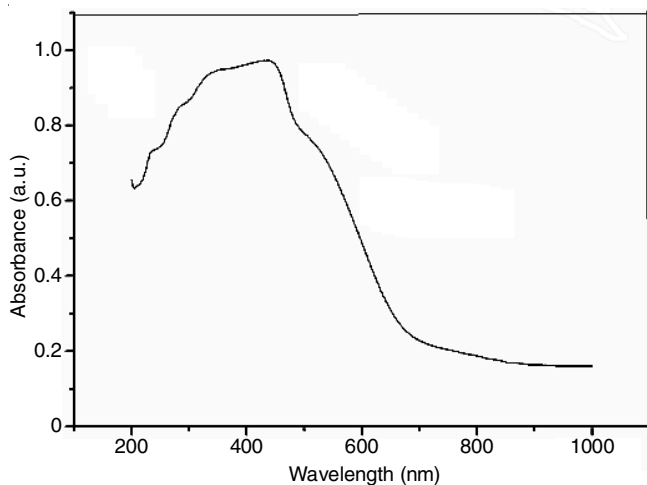


Fig. 7. UV-visible absorbance spectrum of synthesized MNBA compound

(LUMO) separation. This arises due to significant degree of inter/intra molecular charge transfer from the electron-donor to the efficient electron acceptor group through π -conjugated path. HOMO-LUMO plot of MNBA molecule is shown in Fig. 8 from which, it could be inferred that HOMO of π -nature is mainly delocalized over the aromatic C=C part of 4-methylaniline and 2-nitrobenzaldehyde moieties and CH₃ group (push) and imine linkage. In LUMO, an electron density was spread over the C=C part, NO₂ (pull) group of 2-nitrobenzaldehyde moiety only. HOMO→LUMO transition implies that an electron density was transferred from aromatic ring of the 4-methylaniline moiety to nitro group of 2-nitrobenzaldehyde moiety through the single-double bond path in the conjugated bridge involved in push-pull mechanism. Calculated energy values of HOMO and LUMO in gas phase were -6.7024 eV and 4.11194 eV, respectively with energy gap 2.590 eV. HOMO

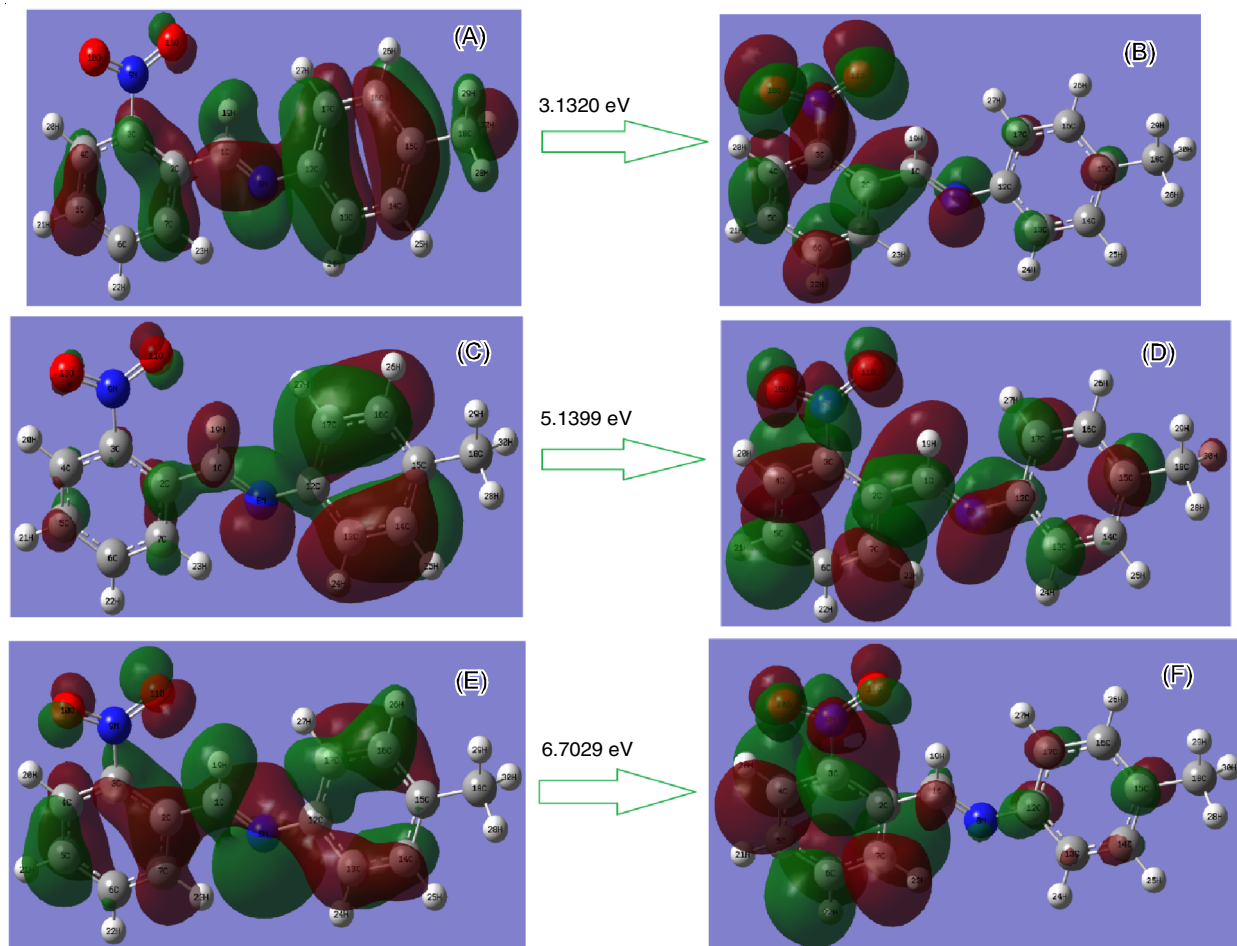


Fig. 8. HOMO LUMO orbitals of MNBA molecule (A), HOMO (B), LUMO (C), HOMO-1 (D), LUMO+1 (E), HOMO-2 and (F) LUMO+2

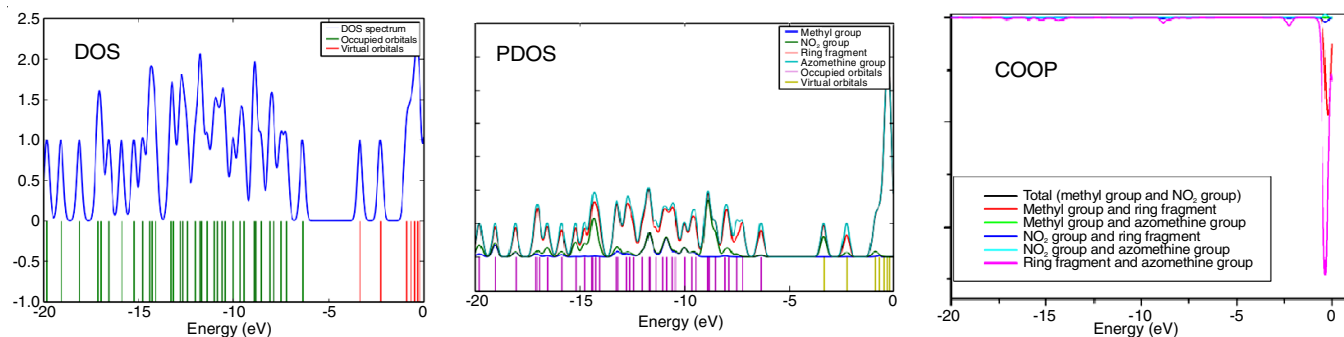


Fig. 9. DOS, PDOS and COOP diagrams of MNBA molecule

→LUMO transition implies an electron density transfer from the highly aromatic part of π -conjugated system to the electron withdrawing NO_2 group. Energy gap between HOMO and LUMO determines the kinetic stability, chemical activity, optical polarizability and chemical hardness-softness of the molecule. Moreover, lower HOMO and LUMO energy gap explains the eventual charge transfer interaction taking place within the system.

Global reactivity descriptors: The global chemical reactivity descriptors of molecules such as hardness (η), chemical potential (μ), softness (S), electronegativity (χ), electrophilicity index (ω) can be determined using HOMO and LUMO energy values and additional electronic charge ΔN_{max} have been defined [36]. Calculated values are shown in Table-7. Group contributions to the density of state (DOS) are given in Fig. 9. When there is a large HOMO-LUMO gap, the molecule is a hard molecule and when the energy gap is small then it is a soft molecule. Stability of molecule and hardness can be related such that the molecule with least HOMO-LUMO gap is more reactive and less stable.

TABLE-7
CALCULATED ENERGIES VALUES OF
SYNTHESIZED MNBA MOLECULE

E_{HOMO}	-6.7024 eV
E_{LUMO}	4.11194 eV
$E_{\text{HOMO}}-E_{\text{LUMO}}$	2.590 eV
Ionisation potential (I)	-6.7024
Electron affinity (A)	4.11194
Hardness (η)	-5.4071
Chemical potential (μ)	1.2952
Softness (ζ)	2.7035
Electronegativity (χ)	5.1809
Electrophilicity index (ω)	0.1551
Additional electronic charge ΔN_{max}	0.2395

Charge analysis

Atomic charge analysis: A charge distribution of MNBA molecule is shown in Fig. 10, while its histogram is given in Fig. 11. Charge distribution within various part of MNBA molecule was calculated in order to understand the reactivity site. Charge analysis revealed that the presence of two electronegative oxygen atoms imposes large positive charge on the nitrogen atom N8 of the nitro group. But atom N11 has highest negative value due to its utmost contribution towards charge delocalization which clearly spells out that the intramolecular charge transfer occurred through this nitrogen atom. Positive charge

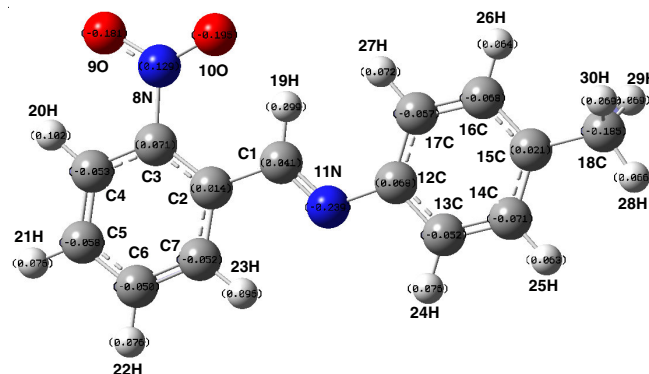


Fig. 10. Mulliken charge distribution of MNBA molecule

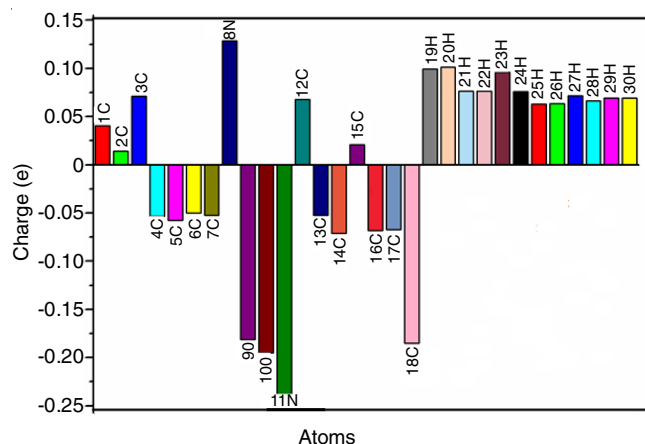


Fig. 11. Mulliken charge distribution for MNBA molecule

on carbon atoms C11, C8, C1, C2 and C3 is a clear evidence for intramolecular charge transfer (ICT), and it indicates the direction of charge transfer from donor moiety 4-methylaniline to acceptor 2-nitrobenzaldehyde through $\text{C1}=\text{N2}$ path. Negative charge on atom C14 indicates its ionic nature. Negative charges on other phenyl ring carbon atoms show its conjugation. All hydrogen atoms of MNBA molecule have positive values (Table-8). Among these, atoms H19 and H20 showed highest positive value due to the highest contribution towards delocalization and their values are equal to 0.10 eV.

Electrostatic potential analysis: Electrophilic reactivity is indicated by red, orange and yellow regions in the MEP map (Fig. 12). Maximum negative region is localized over nitro group, methyl-substituted phenyl ring and the nitrogen atom in the $\text{C}=\text{N}$ group oxygen while the maximum positive region is localized on CH_3 group and $\text{C}-\text{H}$ bonds indicating a possible

TABLE-8
NATURAL CHARGES OF SYNTHESIZED MNBA MOLECULE

Atoms	Charge	Atoms	Charge
C1	1.4782	C16	1.2303
C2	1.2816	C17	1.2333
C3	1.0901	C18	1.405
C4	1.4105	H19	1.4047
C5	1.4068	H20	1.3893
C6	1.396	H21	1.0854
C7	1.4736	H22	1.4039
N8	1.3896	H23	1.0873
N9	1.0825	H24	1.4004
O10	1.3983	H25	1.5098
O11	1.0851	H26	1.3932
C12	1.3893	H27	1.087
C13	1.0857	H28	1.0857
C14	1.0839	H29	1.096
C15	1.4064	H30	1.0964

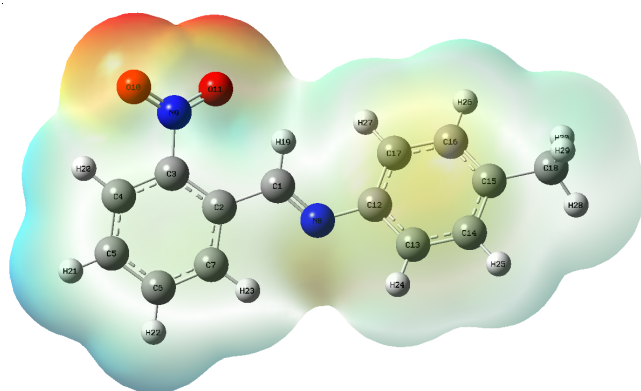


Fig. 12. MEP of MNBA molecule

site for nucleophilic attack. In most of MEPs, red colour indicates the maximum negative region, which was the preferred site for electrophilic attack. So, an approaching electrophile gets attracted to highly negative regions, where electron distribution effect was dominant. From MEP, it is evident that C=O groups has negative charge and the rings and NH group had positive charge.

Antimicrobial activity: 4-Methyl-(2-nitrobenzylidene)aniline was also tested for its antimicrobial activity against human pathogens of clinical isolates (*Salmonella paratyphi*, *Shigella sp.*, *Staphylococcus aureus*, *Streptococcus pyogenes* and *Klebsiella pneumonia*). It showed a maximum zone of inhibition of 17 mm exhibited by *Salmonella paratyphi* (Table-9). The least diameter of zone of inhibition 14 mm was showed by *Shigella sp.*

TABLE-9
ANTIMICROBIAL ACTIVITY OF
SYNTHESIZED MNBA COMPOUND

Microorganism	Zone of inhibition (mm)
<i>Salmonella paratyphi</i>	17
<i>Klebsiella pneumoniae</i>	15
<i>Staphylococcus aureus</i>	15
<i>Streptococcus pyogenes</i>	16
<i>Shigella sp.</i>	14

Auto-docking analysis: Fig. 13 shows a different inhibitor-residue interaction using molecular docking. In molecular docking of protein-ligands residue interaction, energy for the selected proteins are 1BB6, 1CX2, 4ENX and 3VQ7. Binding energies (kcal/mol), bond distances (Å), Reference RMSD (Å) and inhibition constants (M) had also obtained and tabulated in Table-10. Protein-ligands interaction energies of four common residues have a lowest binding energy among these 4ENX had very low binding energy (-4.69 kcal/mol) which was binded with N-H and N-O moieties. This result showed that 4ENX has been the ligand for all the conformations to evaluate the suitability relationship with its antibacterial activity.

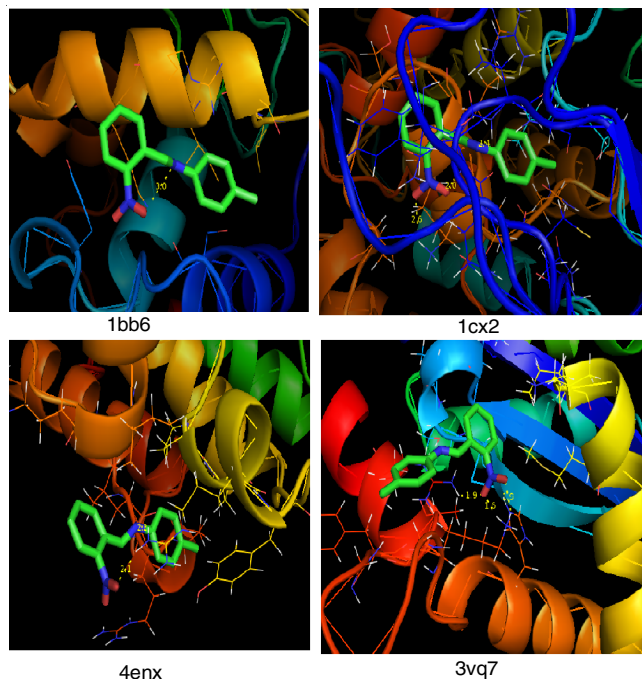


Fig. 13. MNBA molecule docked into the binding site of 1BB6, 1CX2, 4ENX and 3VQ7

TABLE-10
HYDROGEN BONDING AND MOLECULAR DOCKING RESULTS OF
VARIOUS PROTEIN TARGETS WITH SYNTHESIZED MNBA COMPOUND

Protein (PDB ID)	Bonded residues	Number of hydrogen bond	Bond distance (Å)	Estimated inhibition constant (μM)	Binding energy (kcal/mol)	Reference RMSD (Å)
1bb6	TRP	1	3.0	99.29	-5.46	45.96
1cx2	ASN	3	2.6	13.24	-6.65	27.9
	GLU ALA		2.0 2.4			
4enx	ASP	2	2.1	362.1	-4.69	36.91
	ARG		2.2			
3vq7	ARG	3	1.9	29.2	-6.19	31.34
	HIS		1.9			
	LYS		1.6			

Conclusion

A grown compound 4-methyl-(2-nitrobenzylidene)aniline (MNBA) was optimized using DFT (B3LYP) method with 6-311 G(d,p) basis sets. Bond length values of N1-O1 and N1-O2 lie between N-O single and N=O double bond length values, indicating electron delocalization within NO₂ group. The π -electron transfer from the electron donor to acceptor can make the molecule highly polarized. From NBO results, it was clear that pure *p*-type lone pair orbital participating in electron donation was very close to $\sigma^*(\text{N-C})$ orbital for $n(\text{O}) \rightarrow \sigma^*(\text{N-C})$, interactions in MNBA molecule. A C-C stretching bands intensities increases due to the methyl group substituent having electron-donor properties. Downward shifting of C=N stretching frequency was due to charge transfer interaction between the donor and acceptor through -C=N-C skeleton. A 4ENX protein truly reflects the features of MNBA inhibitors and this can be used as fast and accurate tool to assist discovery of novel antibacterial activity.

CONFLICT OF INTEREST

The authors declare that there is no conflict of interests regarding the publication of this article.

REFERENCES

- S. Leela, K. Ramamurthi and G. Bhagavannarayana, *Spectrochim. Acta A Mol. Biomol. Spectrosc.*, **74**, 78 (2009); <https://doi.org/10.1016/j.saa.2009.05.028>
- G.W. Nuss Jr., N.J. Santora and G.H. Douglas, Sunscreen and Erythema Treating with *N*-benzylidene Anilenes, US Patent US4187317A (1978).
- W. Al Zoubi, S.G. Mohamed, A.A.S. Al-Hamdani, A.P. Mahendradhany and Y.G. Ko, *RSC Adv.*, **8**, 23294 (2018); <https://doi.org/10.1039/C8RA01890A>
- G. Gunasekaran and L.R. Chauhan, *Electrochim. Acta*, **49**, 4387 (2004); <https://doi.org/10.1016/j.electacta.2004.04.030>
- G.D. Batema, M. Lutz, A.L. Spek, C.A. van Walree, G.P.M. van Klink and G. van Koten, *Dalton Trans.*, **43**, 12200 (2014); <https://doi.org/10.1039/C4DT01023J>
- C.A. van Walree, O. Franssen, A.W. Marsman, M.C. Flipse and L.W. Jenneskens, *J. Chem. Soc., Perkin Trans. 2*, 799 (1997); <https://doi.org/10.1039/a604603g>
- G.D. Batema, M. Lutz, A.L. Spek, C.A. van Walree, G.P.M. van Klink and G. van Koten, *Dalton Trans.*, **43**, 12200 (2014); <https://doi.org/10.1039/C4DT01023J>
- A. Kajal, S. Bala, S. Kamboj, N. Sharma and V. Saini, *J. Catal.*, **2013**, 893512 (2013); <https://doi.org/10.1155/2013/893512>
- C.M. da Silva, D.L. da Silva, L.V. Modolo, R.B. Alves, M.A. de Resende, C.V.B. Martins and Á. Fátima, *J. Adv. Res.*, **2**, 1 (2011); <https://doi.org/10.1016/j.jare.2010.05.004>
- S.N. Pandeya, D. Sriram, G. Nath and E. DeClercq, *Eur. J. Pharma. Soc.*, **9**, 25 (1999); [https://doi.org/10.1016/S0928-0987\(99\)00038-X](https://doi.org/10.1016/S0928-0987(99)00038-X)
- M.N. Ibrahim, K.J. Hamad and S.H. Al-Joroshi, *Asian J. Chem.*, **18**, 2404 (2006).
- F.D. Popp, *J. Org. Chem.*, **26**, 1566 (1961); <https://doi.org/10.1021/jo01064a063>
- Z. Cimerman, S. Miljanic and N. Galic, *Croatica Chem. Acta*, **73**, 81 (2000).
- M.J. Frisch, G.W. Trucks, H.B. Schlegel, G.E. Scuseria, M.A. Robb, J.R. Cheeseman, G. Scalmani, V. Barone, B. Mennucci, G.A. Petersson, H. Nakatsuji, M. Caricato, X. Li, H.P. Hratchian, A.F. Izmaylov, J. Bloino, G. Zheng, J.L. Sonnenberg, M. Hada, M. Ehara, K. Toyota, R. Fukuda, J. Hasegawa, M. Ishida, T. Nakajima, Y. Honda, O. Kitao, H. Nakai, T. Vreven, J.A. Montgomery Jr., J.E. Peralta, F. Ogliaro, M. Bearpark, J.J. Heyd, E. Brothers, K.N. Kudin, V.N. Staroverov, R. Kobayashi, J. Normand, K. Raghavachari, A. Rendell, J.C. Burant, S.S. Iyengar, J. Tomasi, M. Cossi, N. Rega, J.M. Millam, M. Klene, J.E. Knox, J.B. Cross, V. Bakken, C. Adamo, J. Jaramillo, R. Gomperts, R.E. Stratmann, O. Yazyev, A.J. Austin, R. Cammi, C. Pomelli, J.W. Ochterski, R.L. Martin, K. Morokuma, V.G. Zakrzewski, G.A. Voth, P. Salvador, J.J. Dannenberg, S. Dapprich, A.D. Daniels, Ö. Farkas, J.B. Foresman, J.V. Ortiz, J. Cioslowski and D.J. Fox, Gaussian Inc., Wallingford CT, Gaussian 09, Revision D.01 (2009).
- T. Sundius, *J. Mol. Struct.*, **218**, 321 (1990); [https://doi.org/10.1016/0022-2860\(90\)80287-T](https://doi.org/10.1016/0022-2860(90)80287-T)
- T. Sundius, *Vib. Spectrosc.*, **29**, 89 (2002); [https://doi.org/10.1016/S0924-2031\(01\)00189-8](https://doi.org/10.1016/S0924-2031(01)00189-8)
- P. Pulay, *Mol. Phys.: An Int. J. Interf. Between Chem. Phys.*, **17**, 197 (1969); <https://doi.org/10.1080/00268976900100941>
- P. Pulay, G. Fogarasi, G. Pongor, J.E. Boggs and A. Vargha, *J. Am. Chem. Soc.*, **105**, 7037 (1983); <https://doi.org/10.1021/ja00362a005>
- E. Runge and E.K.U. Gross, *Phys. Rev. Lett.*, **52**, 997 (1984); <https://doi.org/10.1103/PhysRevLett.52.997>
- M. Petersilka, U.J. Gossmann and E.K.U. Gross, *Phys. Rev. Lett.*, **76**, 1212 (1996); <https://doi.org/10.1103/PhysRevLett.76.1212>
- R. Bauernschmitt and R. Ahlrichs, *Chem. Phys. Lett.*, **256**, 454 (1996); [https://doi.org/10.1016/0009-2614\(96\)00440-X](https://doi.org/10.1016/0009-2614(96)00440-X)
- C. Jamorski, M.E. Casida and D.R. Salahub, *J. Chem. Phys.*, **104**, 5134 (1996); <https://doi.org/10.1063/1.471140>
- W. Kohn, A.D. Becke and R.G. Parr, *J. Chem. Phys.*, **100**, 12974 (1996); <https://doi.org/10.1021/jp9606691>
- R.G. Parr and R.G. Pearson, *J. Am. Chem. Soc.*, **105**, 7512 (1983); <https://doi.org/10.1021/ja00364a005>
- P. Politzer and F. Abu-Awwad, *Theor. Chem. Acc.*, **99**(12), 83 (1998); <https://doi.org/10.1007/s002140050307>
- R. Ditchfield, *J. Chem. Phys.*, **56**, 5688 (1972); <https://doi.org/10.1063/1.1677088>
- K. Wolinski, J.F. Hinton and P. Pulay, *J. Am. Chem. Soc.*, **112**, 8251 (1990); <https://doi.org/10.1021/ja00179a005>
- G.M. Morris, R. Huey, W. Lindstrom, M.F. Sanner, R.K. Belew, D.S. Goodsell and A.J. Olson, *J. Comput. Chem.*, **30**, 2785 (2009); <https://doi.org/10.1002/jcc.21256>
- F.H. Allen, O. Kennard, D.G. Watson, L. Brammer, A.G. Orpen and R. Taylor, *J. Chem. Soc., Perkin Trans. II*, S1 (1987); <https://doi.org/10.1039/P29870000051>
- F. Reti, I. Bertoti, G. Mink and G. Varsanyi, *Solid State Ion.*, **44**, 33 (1990); [https://doi.org/10.1016/0167-2738\(90\)90040-X](https://doi.org/10.1016/0167-2738(90)90040-X)
- B.L. Smith, T.E. Schäffer, M. Viani, J.B. Thompson, N.A. Frederick, J. Kindt, A. Belcher, G.D. Stucky, D.E. Morse and P.K. Hansma, *Nature*, **399**, 761 (1999); <https://doi.org/10.1038/21607>
- G. Treboux, D. Maynaud and J.P. Malrieu, *J. Chem. Phys.*, **99**, 6417 (1995); <https://doi.org/10.1021/j100017a021>
- J. Mohan, Organic Spectroscopy Principles and Applications, Narosa Publishing House: New Delhi (2009).
- H.O. Kalinowski, S. Berger and S. Braun, Carbon-13 NMR Spectroscopy, John Wiley & Sons: Chichester (1988).
- K. Pihlaja and E. Kleinpeter, Carbon-13 Chemical Shifts in Structural and Stereochemical Analysis, VCH Publishers: Deerfield Beach (1994).
- A.A. El-Bindary, S.A. El-Korashy, J.A. Hasanen, I.M. El-Deen, M.A. Hussien and S.M. Al-Sayed, *Int. J. Scient. Eng. Res.*, **5**, 851 (2014).